Cloud liquid water path variations with temperature observed during SHEBA experiment

Bing Lin[*1], Patrick Minnis[1], and Alice Fan[2]

[1]Atmospheric Sciences Research

NASA Langley Research Center, Hampton, VA

[2]Science Applications International Corporation, Hampton, VA

Accepted by *Journal of Geophys. Res.-Atmosphere*

December 2002

[*]Corresponding author address: Bing Lin, MS 420, NASA Langley Research Center, Hampton, VA 23681-2199, email b.lin@larc.nasa.gov

Abstract.

Because clouds play such a significant role in climate, understanding their responses to climatic temperature changes is essential to determining the overall impact of a given climate forcing. Cloud liquid water path *LWP* over tropical and midlatitude oceans has been observed to decrease with increasing cloud temperature. The presence of an ice sheet over the Arctic Ocean alters the energy and moisture exchange between the ocean and the atmospheric boundary layer and thus may affect the relationship between *LWP* and temperature. The variations of *LWP* with cloud and surface temperatures are examined in this paper using a combination of surface and satellite data taken during the 1998 Surface Heat Budget of the Arctic Ocean and the FIRE Arctic Clouds Experiments. The results show that *LWP* increases with temperature primarily because of an increase in cloud thickness that is enabled by the rise in surface moisture during the melt season. Cloud-base heights and lifting condensation levels decrease as a result of the greater surface relative humidity and temperature. The average change rate of *LWP* with cloud temperature is 3.3% /K, a value slightly smaller than earlier observations taken over cold mid-latitude land areas. This cloud *LWP* feedback with temperature differs significantly from that estimated over other marine environments and should be taken into account in all climate models with explicit cloud feedbacks.

1. Introduction

For decades, it has been recognized that the variations of cloud properties, such as fractional coverage, temperature, optical depth, particle size and shape, water path, height, and thickness, have an important impact on climate. However, many interactions of clouds within the climate system are not well understood nor accurately characterized. For example, the relationship between tropical high clouds and sea surface temperature and the resultant effects on radiation and climate are so hard to measure that many controversial arguments have been made [*Ramanathan and Collins*, 1991; *Lindzen et al.*, 2001; *Hartmann and Michelsen*, 2002; *Lin et al.*, 2002]. On decadal time scales, the observed variations of tropical radiation fields and the clouds associated with the Hadley and Walker circulations are far beyond global circulation model (GCM) predictions [*Chen et al*., 2002; *Wielicki et al*. 2002]. In polar regions, cloud water path and precipitation rate are very hard to simulate even using single column models [e.g., *Zhang et al.*, 2002].

Cloud observations and analysis of their interactions are also somewhat limited. To date, most cloud feedback observations have focused on low clouds, specifically low-cloud liquid water path *LWP* or its directly associated parameter, optical depth. *Del Genio and Wolf* [2000] extensively investigated the temperature dependence of cloud water path for midlatitude low clouds using ground-based measurements obtained by the Atmospheric Radiation Measurement (ARM) Program at its Southern Great Plains (SGP) site. They found that during summer seasons, cloud water path decreases strongly with increasing temperature, which is consistent with findings from studies of satellite observations at the same latitudes [*Tselioudis et al.*, 1992; *Tselioudis and Rossow*, 1994]. Their results are significantly different from aircraft

measurements over the former Soviet Union [*Feigelson*, 1978] where cloud water content (and path) was usually observed to increase with temperature. The different tendencies suggest that the low-level clouds in cold and warm regions belong to different categories. Based on satellite data, *Tselioudis et al.* [1992] suggested that the temperature T dependence of cloud optical depth OD in cold ($T < 0°C$) and warm ($T > 0°C$) environments could differ in magnitude and even in sign. Additional substantiating evidence for this reverse tendency is scarce because the satellite data only covered latitudes equatorward of 60° due to the large uncertainties in retrieving OD over snow. In polar regions, the temperatures are generally close to or colder than the freezing point even during warm seasons [e.g. *Minnis et al.*, 2001], conditions that are similar to those during the aircraft measurements in former Soviet Union [*Feigelson*, 1978]. Over the Arctic ice pack, the albedo contrast between boundary layer clouds and snow/pond-covered surfaces has a strong influence on the distribution of solar radiation [*Curry et al.*, 1996]. The radiative feedback of these stratus clouds is mainly governed by the macro- and microphysical properties of the clouds, especially cloud water path and particle size and shape [*Stamnes et al.*, 1999]. The variations in cloud properties with changes in temperature play a fundamental role in the cloud-radiative feedback system. Thus, it is important to more accurately quantify the sensitivity of Arctic stratus clouds to changes in the cloud temperature.

Accurate retrieval of OD over snow surfaces is extremely difficult from most satellite imagers. However, by combining ground-based data with satellite observations, it is possible to obtain a better measure of cloud properties including OD and LWP. A unique set of measurements was taken from the Arctic ice pack for an entire year (October 1997 - October 1998) by the Surface Heat Budget of the Arctic Ocean (SHEBA) project [*Uttal et al.*, 2002].

A more intensive study of Arctic clouds and radiation using aircraft, surface, and satellite measurements was conducted in conjunction with SHEBA by the First ISCCP Regional Experiment Arctic Cloud Experiment (FIRE ACE) during May through July 1998 [*Curry et al.*, 2000]. Data from these two sources provide an unprecedented opportunity for examining a variety of previously intractable cloud-radiative phenomena in the Arctic Basin. This paper uses a variety of measurements taken during those campaigns to investigate the dependence of cloud liquid water path on temperature in the Arctic region.

2. Data and retrieval algorithms

As part of the comprehensive observational program, the Atmospheric Radiation Measurement Program deployed an uplooking microwave radiometer (MWR) at the SHEBA site [*Stamnes et al.*, 1999]. The MWR measured downwelling radiances at frequencies of 23.8 and 31.4 GHz every 20 seconds, and had automatic self-calibration capability with an accuracy within 0.3 K in measured brightness temperature *Tb* (i.e., radiance). The calibrated data were recorded every 2 minutes. Cloud liquid water path and column water vapor (*CWV*) were retrieved from the calibrated MWR measurements using the algorithm developed by *Lin et al*. [2001]. This algorithm is adopted from the satellite remote sensing technique of *Lin et al.* [1998b], and properly accounts not only for the temperature and pressure dependence of atmospheric gas absorption at the microwave wavelengths, but also the variation of water absorption with the cloud water temperature [*Lin et al*., 1998a; *Lin et al*., 2001]. The vertical distributions of temperature, pressure and water vapor abundance were constructed based on climatological profiles interpolated to conform to the SHEBA ground meteorological

measurements and assumed *CWV*, respectively. During retrieval, *LWP* and *CWV* values were iteratively adjusted so that *Tb* computed with the microwave radiative transfer model matched *Tb* measured with the MWR. A by-product of the retrieval is cloud-base temperature measured by the Infrared Thermometer (IRT). To be consistent with the MWR data, the original IRT 1-minute samples were averaged to 2-minute temporal resolution values. The uncertainty for *LWP* retrieval is <0.02 mm [*Lin et al*., 2001]. Compared with in situ aircraft *LWP* measurements made during FIRE ACE, the MWR technique results differed by only 3% from the averaged in situ *LWP* [*Lin et al*., 2001]. The root mean square (rms) *LWP* errors are about 0.024 mm (or 25%), which is larger than the uncertainties in the retrieval algorithm. The spatial and temporal mismatches between MWR retrievals and in situ measurements probably contribute significantly to the rms errors. Thus, the *Lin et al*. [2001] algorithm should provide accurate *LWP* retrievals for the variety of temperatures observed in Arctic clouds.

Air temperature (*Ta*), pressure, relative humidity, and other meteorological parameters were measured at 2 m on two SHEBA towers and reported hourly as the average of the two tower observations. The hourly data were interpolated to match the MWR measurement times when needed. Cloud top and base heights were estimated from the cloud-top and base temperatures derived from NOAA-12 and NOAA-14 Advanced Very High Resolution Radiometer (AVHRR) data [*Minnis et al*., 2001] and ground-based IRT thermal infrared (IR) measurements, respectively, with SHEBA atmospheric profile information. These estimated cloud heights were found to be consistent with SHEBA radiosonde observations using a technique similar to *Wang et al*. [2000].

Since cloud heights and boundaries were also estimated from the NOAA Environmental Technology Laboratory millimeter cloud radar (MMCR) for every 10 seconds [*Minnis et al*., 2001], the cloud heights from the IR techniques were compared with the radar retrievals. Although a combination of lidar and radar measurements can provide reasonable detection of cloud boundaries [*Clothiaux et al*., 2000], the MMCR cloud height data used here was measured by radar only. Comparison revealed significant differences between the cloud heights estimated from passive (satellite or ground-based IR measurements) and active (radar) techniques. During the FIRE ACE period, analyses of the MMCR data showed that about 64% of the radar-measured atmospheric profiles had cloud bases at the first available radar gate above ground (105 m), which were not apparent in the IRT data and sounding profiles. Furthermore, the cloud-top heights estimated from the MMCR were about 60% higher than those derived from satellite measurements using soundings of vertical temperature profiles. Figure 1 plots the collocated radar and AVHRR-based cloud-top heights within 30 minutes centered at satellite overpasses and 25-km radius around the site, respectively. The correlation (coefficient 0.54) is significantly positive with statistical confidence above 99%. On average, the satellite estimates are about 1.7 km lower than the radar values. The bias is primarily due to the occurrence of overlapped clouds, i.e., thin cirrus over stratus. The high-cloud optical depths were often too small to cause much of a change in the AVHRR brightness temperature so that the observed temperature is close to that of the underlying stratus clouds. Because the low-level stratus clouds are so prevalent [*Minnis et al.*, 2001], the cirrus clouds often occurred at the same time as the stratus clouds. Other sources for the average difference include the lack of sufficient resolution in the temperature profiles used to convert the cloud temperatures to

altitudes and difficulties in identifying thin cirrus and correcting for its semi-transparency in the AVHRR data even when no stratus clouds were present.

When the uppermost clouds were optically thick, the MMCR and AVHRR results of cloud top height are usually in good agreement. At low altitudes, $z < 4$ km, the radar and AVHRR retrievals are also in relatively good agreement (Fig. 1). The mean difference between the two measurements is 0.1 km with standard deviation 1.0 km and correlation coefficient 0.64. Because this study focuses on the *LWP* temperature dependence and most of the liquid-water clouds are at low levels, the cloud heights and temperatures retrieved from AVHRR and ground-based passive IR measurements were used. The averaged satellite results of cloud top temperature, cloud-top height and cloud fraction within a 25-km radius around the site were collocated with ground-based measurements within 30 minutes centered at the time of the satellite overpasses. The MMCR images were used to manually separate single-layer from multiple-layer clouds to classify the satellite observations. Note that for general MWR *LWP* retrievals, especially for *LWP* values obtained when AVHRR were not available, this classification process of single and multi-layer clouds was not applied due to limited manpower and the huge data volume.

Although *LWP* was retrieved from the operational MWR data for the entire SHEBA time period, the full suite of ground-based and spaceborne instruments were only available during FIRE ACE. Due to this limitation, this study uses both the full suite of data sets during FIRE ACE and some partial data sets of pertinent cloud parameters during the remainder of SHEBA. To further verify the relationship of cloud *LWP* and temperature, 10-minute averaged cloud-base height estimates from the SHEBA Depolarization and Backscatter Unattended Lidar

(DABUL; [Alvarez et. al., 1998]) were also analyzed. The DABUL data provide the opportunity to separate liquid and ice phase clouds [Sassen, 1991] and to detect single and multi-layer clouds as long as the lidar signals are not attenuated. The current study uses only cloud-base heights for single-layered water clouds (absolute depolarization ratio < 0.05). Comparison of the IRT and lidar cloud-base heights shows that the two techniques yield consistent results with a statistically significant correlation and a 0.4-km mean difference with a 0.5-km standard deviation. The IRT height should be greater than the DABUL value because the latter measures the physical cloud base while the former corresponds to the effective radiating level, which should be at some depth in the cloud. Cloud-top height data are not used to avoid the lidar pulse stretch and attenuation problems since our analysis only considers clouds with *LWP* larger than 0.02 mm (or *OD* >~3).

3. Results

The average cloud coverage over the SHEBA ice camp was generally 65% or greater year around [*Zhang et al*., 2002]. During most of the SHEBA experiment, the clouds were almost entirely composed of ice. The *LWP* derived from the MWR data was close to zero nearly every day during the winter (December 1997 to March 1998) as a result of the extreme cold (c.f. Fig. 11 of *Zhang et al*.). Significant amounts of liquid water were not observed until the spring thaw was well underway (i.e., May 1998). Figure 2 shows a scatter plot of all derived *LWP* and the cloud base temperature *T* values from May through July 1998 (i.e., FIRE-ACE period). Because of the instantaneous uncertainties (< 0.02 mm) in the MWR retrievals, only data with *LWP* > 0.02 mm are used to ensure that the signal-to-noise ratio

exceeds unity. With that threshold, some thin clouds are likely to be eliminated in the analysis, but the risk of falsely detected water clouds is also significantly reduced. Clearly, the data can be separated into two branches: stratiform clouds with small (<~0.15 mm) *LWP* values and some disturbed cases with larger *LWPs* that are probably associated with precipitation systems. In both branches, *LWP* significantly increases with cloud water temperature.

The significant increase of *LWP* with cloud temperature is also evident in the smaller data set of matched satellite and ground-based observations (i.e., the full suite of data sets). The AVHRR data analyzed by *Minnis et al.* [2001] were taken over the ice camp roughly 4 - 8 times each day resulting in 496 matched cases during FIRE ACE. After applying the 0.02-mm threshold, only 259 water cloud cases were available. Of these, 115 and 133 were classified as most cloudy (100% > cloud cover > 50%) and overcast cases, respectively, by satellite remote sensing. Figure 3 shows the relationships between *LWP* and cloud height for overcast cases. (Note: the results using all 259 cases are very similar to the overcast cases in Figure 3.) Generally, *LWP* increases with increasing cloud-top height (3a) and with decreasing cloud-base height (3b). Although the relationship between *LWP* and cloud-top height is not as strong as that for *LWP* and cloud-base height, both correlations are reasonably high (the absolute values of the coefficients were 0.3 - 0.4) and statistically significant with confidence levels above 99%. Because of the rather stable lapse rates during the FIRE-ACE period, when satellite cloud-top temperature (or ground-based IRT cloud-base temperature) values are analyzed, the *LWP* variations with the cloud temperatures are almost the same as those with cloud-top height (or cloud-base height) shown in Fig. 3a (or 3b), except with opposite trends. Thus, increasing cloud thickness is mainly responsible for the enlarged *LWP* (Figure 3c). The

points with small (<~0.1 mm) *LWP* values and high (>~4 km) cloud tops or large cloud thickness are probably mixed-phase or overlapped clouds. It is emphasized that even though some of them are thin and mixed-phase, the clouds analyzed here should possess the general characteristics of water clouds since the *LWP* values of these clouds are significantly larger than or, at least, close to the aircraft in situ observations taken during FIRE ACE [Lin et al., 2001]. Actually, for thicker water clouds (i.e., a *LWP* threshold 0.05 mm, which is equivalent to an *OD* of about 7, is used to remove all thin water clouds), *LWP* trends similar to those in Figs. 2 and 3 are also observed.

Although the changes in *LWP* are significantly related to cloud height and thickness, these vertical structures of the low clouds, which are generally correlated with local atmospheric temperature and humidity (see discussions later), can only explain some of the *LWP* variations. Many other factors, such as small-scale turbulence, large-scale atmospheric dynamics, cloud particle phase, and multi-layer cloud systems, can affect cloud water path. Despite the changes in *LWP* with both cloud-top and base heights (or cloud thickness), cloud liquid water content (*LWC*) varies little with *LWP* (Figure 3d). Figure 4 shows the variations of *LWC* with surface air and cloud temperatures. Figures 4a and 4b plot the *LWC* values calculated from *LWP* and the IR-retrieved cloud thickness. When the cloud thickness values estimated from satellite and ground-based IR measurements are replaced by the MMCR cloud thickness data, the *LWC* results (Figs. 4c and 4d) are almost the same as those from the IR estimates. This further analysis reveals that *LWC* actually did not change significantly with cloud and air temperatures either.

In general, cloud temperature is decoupled from the surface (or environmental) temperature. However, for the cases observed here, cloud temperature is strongly correlated with surface temperature because of the relationship between boundary-layer relative humidity and the temperature. Thus, the *LWP* increase with cloud temperature is also accompanied by an increase in surface temperature (Figure 5) or vice versa. The small number of data points around surface temperatures between 259K and 263K are a result of using only cloud data with $LWP > 0.02$ mm. The original SHEBA meteorological measurements recorded a wide range of surface temperatures with $LWP < 0.02$ mm. When single and multiple layer clouds were determined and separated manually by inspection of MMCR imagers, the dependence of *LWP* on *T* or cloud height (not shown) was generally the same as or more obvious than those seen in Figures 2 and 5. Thus, the decrease in cloud-base heights and the increase in cloud-top heights with increasing temperature were more or less common for the observed Arctic water clouds.

To further confirm the *LWP* variations with cloud temperature, the DABUL cloud-base height data were analyzed. The data show *LWP* changes with the environmental conditions that are very similar to those in Figures 2 and 3. Figure 6 plots the relationship between *LWP* and cloud-base height for all single-layered water clouds detected by the lidar measurements. Potential fog cases (or cases with surface relative humidity $\geq 100\%$) were eliminated from the original DABUL data to avoid clouds with bases lower than the range of the lidar's first gate (or to avoid height detection error caused by lidar minimal range). The figure clearly shows that the *LWP* decrease with increasing cloud-base height is statistically significant. Since the DABUL depolarization ratio is used in the analysis for these single-layered clouds, the results are not

affected by ice clouds, mixed phase conditions, or cloud ice water path (*IWP*) values. The similarity between this figure and Fig. 3b provides not only additional evidence of the increase of *LWP* with *T* but it also shows the consistency of different remote sensing techniques in analyzing cloud properties.

The temperature dependence of *LWP* is also apparent in the monthly mean data. Figure 7 shows two-dimensional histograms of *LWP* and cloud base temperature for May, June and July 1998. The statistics reveal very similar distributions for the 3 months, with the exception of a slight shift in the peak due to the increase in monthly mean cloud-base temperatures. As the cloud temperature increases from 255K to 272K, the magnitude and frequency of *LWP* increases during all 3 months, a strong indication of a dependence of *LWP* on temperature. Furthermore, the peak *LWP* frequency during May was located at about 266 K and 0.045 mm. As the environment warmed, the peaks moved to cloud temperatures around 270K and 271K and *LWP* near 0.05 mm and 0.06 mm in June and July, respectively.

4. Discussion

If the rate of change with temperature for an arbitrary parameter A is f defined as $f(A) = A^{-1}\mathrm{d}A/\mathrm{d}T$, then for the dataset in Figure 2, $f(LWP)$ is about 0.033 /K. Similarly, the rate of change of *LWP*, $f(LWP)$, with cloud-base height obtained from the DABUL data is about −0.19 /km, which corresponds closely to the 0.033 /K f value with temperature obtained from the IRT data if the averaged lapse rate of about −5 K/km observed during the FIRE ACE period is considered. Based on aircraft measurements over the former Soviet Union [*Feigelson*, 1978], *Somerville and Remer* [1984] obtained f values 0.04 ~ 0.05 /K. The

present estimated f value is also close to that of *Tselioudis et al.* [1992], which was estimated over land from midlatitudes at cloud temperatures colder than ~265K, and about a factor of two larger than theirs over ocean. For cloud temperatures greater than ~265 K, especially for temperatures above the freezing point, *Tselioudis et al.* [1992] observed negative f values, while the positive f value, or the increase of cloud water path, continued throughout the full range of cloud temperature in this study, which is similar to the aircraft observations of *Feigelson* [1978]. Over polar ice sheets, the environmental conditions that give rise to cloud formation are considerably different from those over midlatitude oceans, even when the temperatures are similar because of the polar boundary layer dynamics and the sensitivity of the boundary layer humidity to presence of the ice sheet. The *LWP* temperature dependence over the ice sheet has some similarities to that in winter midlatitude land regions, as seen by DelGenio and Wolf [2000]. Both regions have limited heat capacity and column water vapor relative to the ocean. The stronger temperature dependence of *LWP* in disturbed conditions further demonstrates the importance of moisture on clouds, especially on convection. For the disturbed cases, almost all observed cloud temperatures were higher than 260 K. With the relatively warm temperature and unstable conditions, both relative and specific humidity values were increased (see later). Thus, at higher temperatures convergent processes pumped more moisture into atmosphere, and formed thick water clouds.

When *LWP* is averaged for each 1-K temperature interval, as in Figure 7, the estimated f values for these monthly-scale *LWP* changes are about 0.07 /K, which is about two times larger than that (~0.033 /K) estimated from short-time-scale data (c.f. Fig. 2). The assumption for obtaining this stronger cloud feedback factor with temperature is that the water clouds are

equally distributed over the considered temperature range. Similar calculations by *Somerville and Remer* [1984] for temperature-binned cloud water content data from aircraft measurements over the former Soviet Union [*Feigelson*, 1978] also yielded slightly higher f values (0.04 ~ 0.05 /K). For climate studies, the estimation from the original *LWP* samples (c.f. Fig. 2), which is equivalent to cloud water path weighted by cloud population in each temperature bin, may be more realistic.

Although the changes of *LWP* with *T* observed here are similar to the observations of *Feigelson* [1978] and those proposed by *Somerville and Remer* [1984] and *Betts and Harshvardhan* [1987], the present result arises for considerably different physical reasons. The change in cloud thickness, not the *LWC* associated with temperature, caused the rise in *LWP*. The *LWP* change resulting from the cloud thickness variations (both cloud top and base height changes) was also observed by *Del Genio and Wolf* [2000]. However, their results were mainly due to a cloud-base height change with an opposite change of *LWP* with *T* relative to the present result here and their observations were taken over the ARM SGP site, a relatively warm midlatitude land area.

The decrease of cloud-base height with *T* is directly connected to an increase in surface humidity and to a lower cloud lifting condensation level (LCL). Figure 8a shows that as the surface air temperature varied from 255 K to 275 K, the surface relative humidity, though variable for a given temperature, changed on average from ~78% to ~95%. Saturated air for temperatures above the freezing point develops from the abundant moisture available from the melt ponds and melting snow around the ice camp. As surface temperature rose, the specific humidity increased sharply from ~0.7 g/kg to ~4.0 g/kg (Figure 8b) partly due to the nonlinear

Clausius-Clapeyron relationship between temperature and saturation vapor pressure. When lifted and cooled, surface air parcels with elevated surface relative humidity at high temperatures condense water vapor more quickly than those with lower humidity at low temperatures. As a consequence, the LCL of surface air estimated from the SHEBA surface humidities and temperatures and atmospheric vertical profiles decreased from ~0.5 km at low temperatures to altitudes just above or at the surface for warm temperatures (Figure 9). To the first order, the water vapor mixing ratio (ω), in this case the saturation mixing ratio (ω_s), at LCL is the combination of ω_s at surface and the change of ω_s with temperature (or height). Because dry adiabatic lifting process conserves not only potential temperature but also ω, the ω_s at LCL is equal to $rh \times \omega_s$ at surface, where *rh* is relative humidity. Thus, LCL decreases strongly with relative humidity, as shown in Figure 10. Although temporal and spatial differences between remote sensing and sounding measurements can cause differences between the estimated LCL and the observed cloud-base height, the main trends of the two values are basically consistent (Figure 11). This positively correlated feature is very clear when the cloud-base heights are averaged into half-kilometer bins (solid curve in Fig. 11). Higher observed cloud-base heights than those for the estimated LCL may be due to entrainment of dry air into the bottom of the clouds after cloud formation and/or the formation of clouds in air parcels that originated in layers disconnected from the surface. Inversion and non-local dynamic processes such as advection could be another reason for the differences. Large differences between the observed *LWC* and the calculated adiabatic *LWC* further indicate that the cloud base height not *LWC*, especially not the adiabatic *LWC* dependence on temperature, is significantly correlated to temperature and produces the observed *LWP* dependence on temperature. Because of the humidity, again, the

moist static energy of the surface air parcel is higher at warmer rather than lower temperatures, which, at least partly, causes the increase in cloud top heights, especially in moist convection cases. Deepening boundary layers may be another reason for increased cloud-top heights in warm and humid environments. Thus, the cloud physics that causes *LWP* to increase with *T* is the increase of cloud thickness resulting from warmer and moister environments. Tselioudis et al. [1998] showed that the tendency for optical depth to increase with temperature observed by satellite at high latitudes (up to 60°) was reproduced in a GCM primarily because cloud thickness increased with *T*, and that in turn occurred because relative humidity increased with temperature at high latitudes. The current observations confirm the GCM cloud behavior and its physical mechanism in driving *LWP* variations at polar regions.

5. Conclusions

Over the SHEBA site during FIRE-ACE, cloud liquid water path increased with temperature due primarily to an increase of cloud thickness. When temperature rose, both surface specific and relative humidity increased. As a result, the cloud base height (and cloud lifting condensation level) dropped. Although adiabatic cloud water content increased with temperature, this study found no significant cloud water content variation with cloud temperature. The observed temperature dependence of *LWP* was about 3.3% /K, which is slightly smaller than other observations from cold mid-latitude land environments. These observed cloud variations have significant effects on the polar climate. Even within a seasonal time scale, the cloud feedback provides negative effects on the transition from cold to warm seasons because of enhanced reflection of solar radiation. Since only limited data were

analyzed, more studies on longer time and greater space scales, e.g., inter-annual variations of cloud water path on temperature, are needed to determine if these results are representative of polar regions in general. With further confirmation, this cloud *LWP* temperature dependence should be taken into account in all climate models with explicit cloud feedbacks.

Acknowledgements: Discussions with Y. Hu and K.-M. Xu, D. Spangenberg, and A. Cheng are very helpful for this study. This research was supported by NASA Earth Sciences Enterprise FIRE and CERES Projects and by the Environmental Sciences Division of U.S. Department of Energy Interagency Agreement DE-AI02-97ER62341 under the ARM Program.

References

Alvarez, R.J., II, W.L. Eberhard, J.M. Intrieri, C.J. Grund, and S.P. Sandberg, A depolarization and backscatter lidar for unattended operation in varied meteorological conditions. *Proc. of the 10th AMS Sym. on Meteor. Obs. and Instrum*., Phoenix, AZ, 11-16 January, 1998.

Betts, A. K., and Harshvardhan, Thermodynamic constraint on the cloud liquid water feedback in climate models, *J. Geophys. Res., 92*, 8483-9485, 1987.

Clothiaux, E. E., et al., Objective determination of cloud heights and radar reflectivities using a combination of active remote sensors at the ARM CART sites, *J. Appl. Meteorol., 39*, 645-665, 2000.

Curry, J., W. B. Rossow, D. Randall, and J. L. Schramm, Overview of arctic cloud and radiation characteristics, *J. Clim.*, *9*, 1731-1764, 1996.

Curry, J. A., P. Hobbs, M. D. King, D. A. Randall, P. Minnis, T. Uttal, G. A. Isaac, J. O. Pinto et al., FIRE Arctic Clouds Experiment, *Bull. Amer. Meteor. Soc.*, *81*, 5-29, 2000.

Chen, J., B. E. Carlson, A. D. Del Genio, Evidence for strengthening of tropical general circulation in the 1990s, *Science*, *295*, 838-841, 2002.

Del Genio, A. D., and A. B. Wolf, The temperature dependence of the liquid water path of low clouds in the Southern Great Plains, *J. Clim.*, *13*, 3465-3486, 2000.

Feigelson, E. M., Preliminary radiation model of a cloudy atmosphere, Part I, Structure of clouds and solar radiation, *Beitr. Phys. Atmos.*, *51*, 203-229, 1978.

Hartmann, D. L., and M. L. Michelsen, No evidence for iris, *Bull. Amer. Meteor. Soc.*, *83*, 249-254, 2002.

Lin, B., B. Wielicki, P. Minnis, and W. B. Rossow, Estimation of water cloud properties from satellite microwave, infrared, and visible measurements in oceanic environments. I: Microwave brightness temperature simulations, *J. Geophys. Res.*, *103*, 3873-3886, 1998a.

Lin, B., P. Minnis, B. Wielicki, D. Doelling, R. Palikonda, D. Young, and T. Uttal, Estimation of water cloud properties from satellite microwave, infrared, and visible measurements in oceanic environments. II: Results, J. Geophys. Res., 103, 3887-3905, 1998b.

Lin, B., P. Minnis, A. Fan, J. A. Curry, and H. Gerber, Comparison of cloud liquid water paths derived from in situ and microwave radiometer data taken during the SHEBA/FIREACE, *Geophys. Res. Lett.*, *28*, 975-978, 2001.

Lin, B., B. Wielicki, L. Chambers, Y. Hu, and K.-M. Xu, The Iris hypothesis: A negative or positive cloud feedback? *J. Clim.*, *15*, 3-7, 2002.

Lindzen, R., M.-D. Chou, and A. Hou, Does the Earth have an adaptive infrared iris? *Bull. Amer. Meteor. Soc.*, *82*, 417-432, 2001.

Minnis, P., et al., Cloud coverage and height during FIRE ACE derived from AVHRR data, *J. Geophys. Res.*, *106*, 15215-15232, 2001.

Sassen, K., The polarization lidar technique for cloud research: A review and current assessment, *Bull. Amer. Meteor. Soc*., 72, 1848-1866, 1991.

Somerville, R. C. J., and L. A. Remer, Cloud optical thickness feedback in the CO2 climate problem, *J. Geophys. Res.*, *89*, 9668-9672, 1984.

Perovich, D. K., and coauthors, Year on ice gives climate insights, *Eos, Trans. AGU*, *80*, 481, 1999.

Ramanathan, V., and W. Collins, Thermodynamic regulation of ocean warming by cirrus clouds deduced from observations of the 1987 El Nino, *Nature*, 351, 27-32, 1991.

Stamnes, K, R. G. Ellingson, J. A., Curry, J. E. Walsh, and B. D. Zak, Review of science issues, development strategy, and status from the ARM North Slope of Alaska-adjacent Arctic Ocean climate research site, *J. Clim.*, *12*, 46-63, 1999.

Tselioudis, G., A.D. DelGenio, W. Kovari, and M.-S. Yao, Temperature dependence of low cloud optical thickness in the GISS GCM: Contributing mechanism and climate implications, *J. Clim*., *11*, 3268-3281, 1998.

Tselioudis, G., and W. B. Rossow, Global, multiyear variations of optical thickness with temperature in low and cirrus clouds, *Geophys. Res. Lett*., *21*, 2211-2214, 1994.

Tselioudis, G., W. B. Rossow, and D. Rind, Global patterns of cloud optical thickness with temperature, *J. Clim.*, *5*, 1484-1495, 1992.

Uttal, T., et al., Surface Heat Budget of the Arctic Ocean, *Bull. Amer. Meteor. Soc.*, *83*, 255-276, 2002.

Wang, J., and W. B. Rossow, Y. Zhang, Cloud vertical structure and its variations from a 20-yr global rawinsonde dataset, *J. Clim.*, *13*, 3041-3056, 2000.

Wielicki, B. A., et al., Evidence for large decadal variability in the tropical mean radiative energy budget, *Science, 295*, 841-844, 2002.

Zhang, J., U. Lohmann, and B. Lin, A new statistically based autoconversion parameterization for use in larger-scale models, accepted by *J. Geophys. Res.*, 2002.

Figure Captions

Figure 1. Scatter plot of MMCR estimated cloud top height with satellite estimated cloud top height.

Figure 2. The relationship between cloud liquid water path (*LWP*) and cloud base temperature.

Figure 3. *LWP* dependence on cloud top height (a), cloud base height (b), cloud thickness (c) and cloud liquid water content *LWC* (d).

Figure 4. Scatter plot of *LWC* with surface temperature (a) and cloud base temperature (b). The panels c and d are the same as panels a and b, respectively, except the cloud thickness data from MMCR are used in *LWC* calculations.

Figure 5. Same as Figure 2, except for surface air temperature.

Figure 6. The relationship between *LWP* and cloud base height observed by DABUL.

Figure 7. Statistics on *LWP* and cloud base temperature for May, June and July 1998.

Figure 8. Surface air temperature dependence of relative humidity (a) and specific humidity (b).

Figure 9. Temperature dependence of cloud lifting condensation level (LCL). The LCL values were theoretically estimated from surface meteorological measurements of temperature and humidity and atmospheric profile.

Figure 10. Theoretically estimated LCL for different relative humidities in the surface air temperature range from 255K to 275K.

Figure 11. Scatter plot of LCL and observed cloud base height. The solid curve is for the averages of cloud base height binned in every half-kilometer.

Figure 1

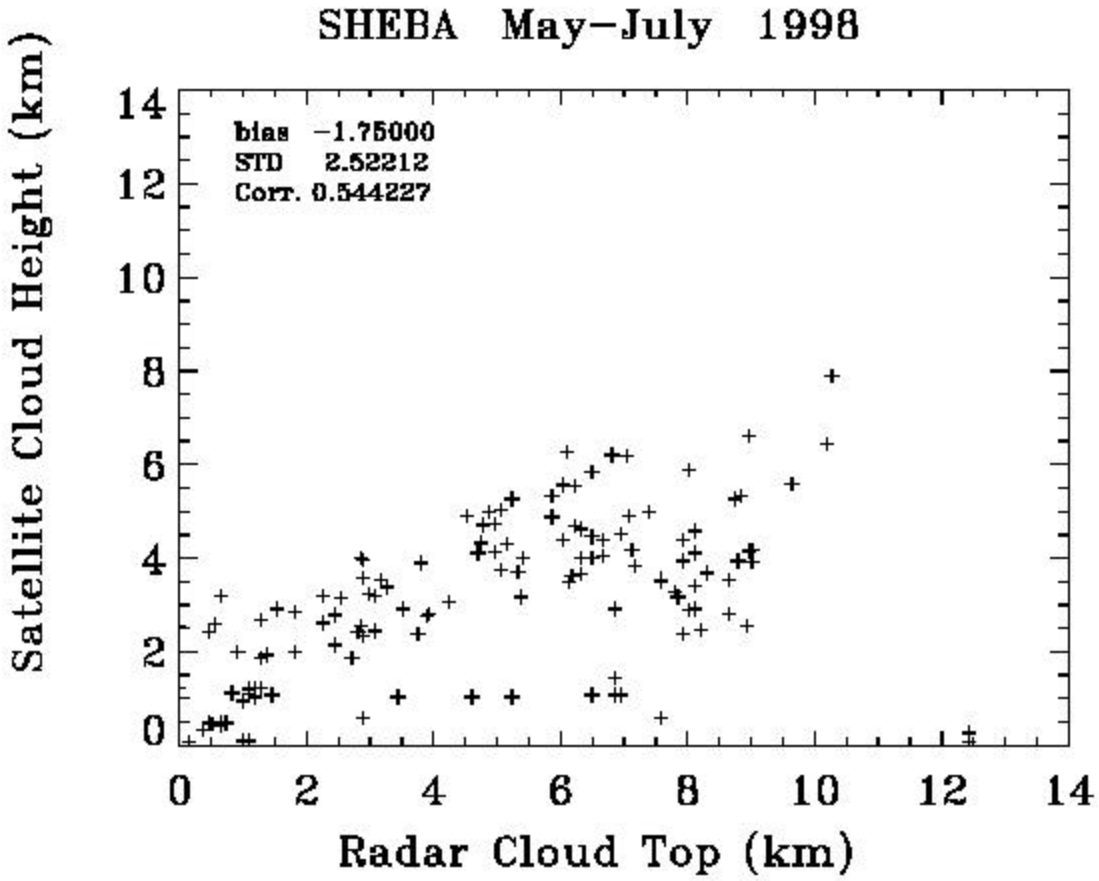
SHEBA May−July 1998
bias −1.75000
STD 2.52212
Corr. 0.544227
Satellite Cloud Height (km)
Radar Cloud Top (km)
0
2
4
6
8
10
12
14

Figure 2

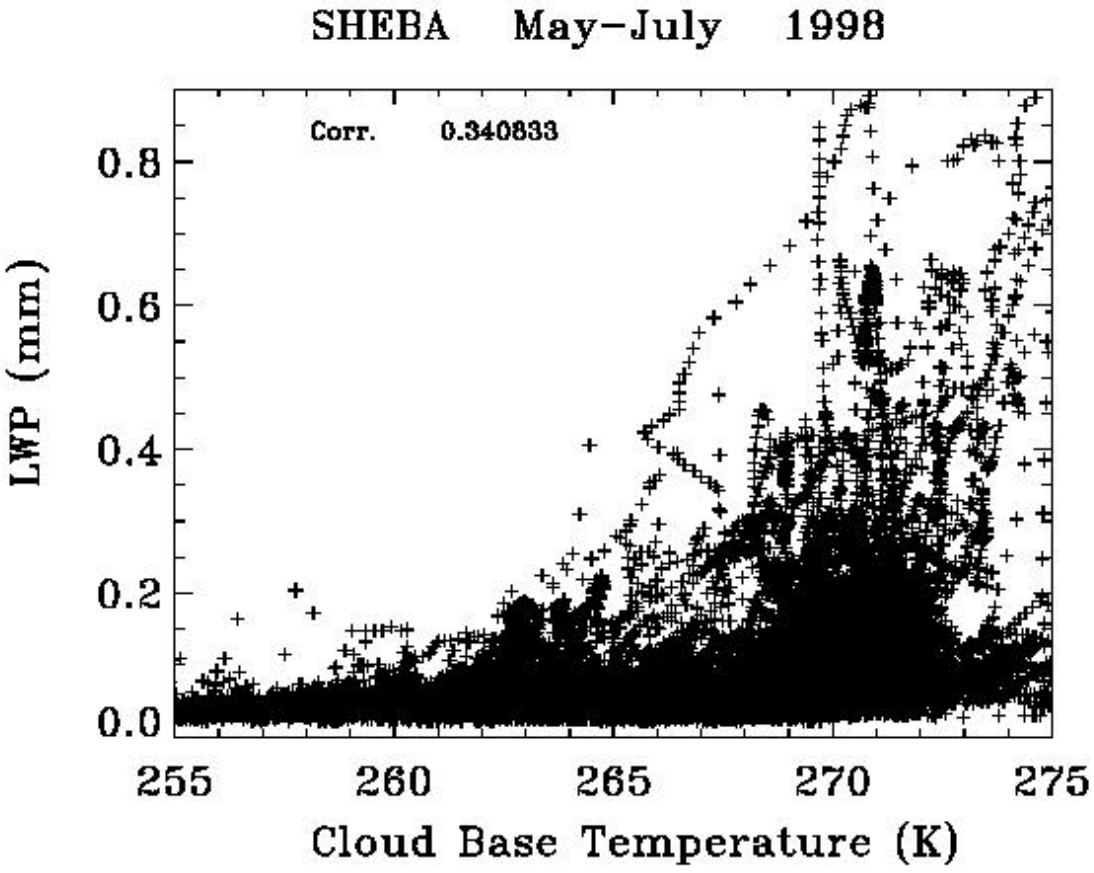
SHEBA May–July 1998
Corr. 0.340833
LWP (mm)
0.0
0.2
0.4
0.6
0.8
255
260
265
270
275
Cloud Base Temperature (K)

Fig. 3

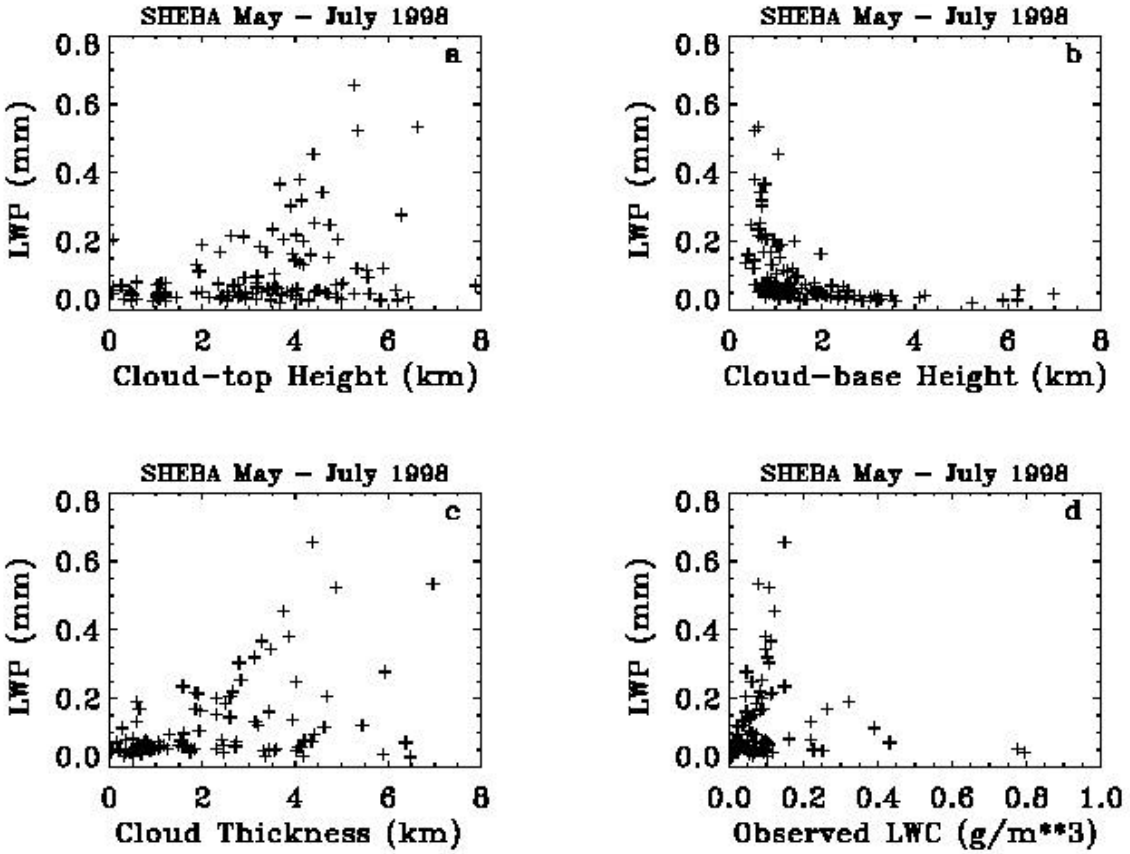
SHEBA May – July 1998
a
LWP (mm)
Cloud–top Height (km)
SHEBA May – July 1998
b
LWP (mm)
Cloud–base Height (km)
SHEBA May – July 1998
c
LWP (mm)
Cloud Thickness (km)
SHEBA May – July 1998
d
LWP (mm)
Observed LWC (g/m**3)

Fig. 4

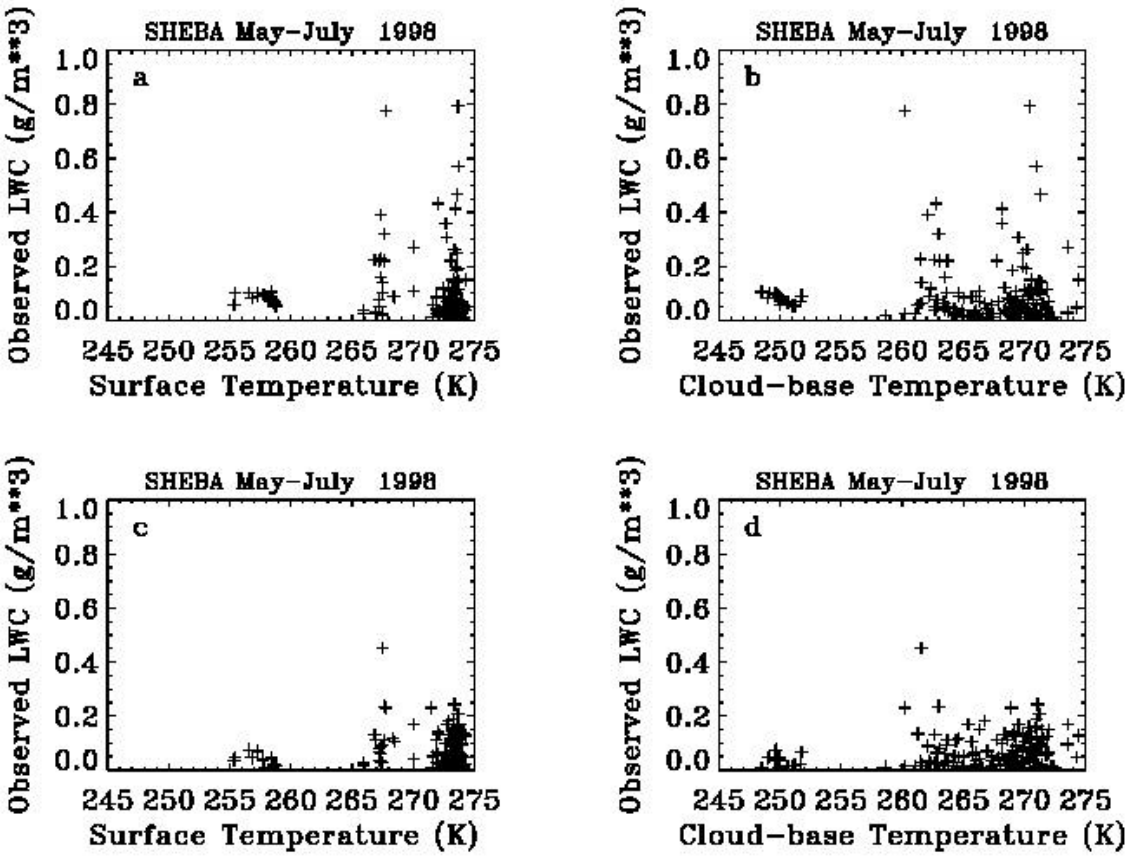
SHEBA May–July 1998
a
Observed LWC (g/m**3)
1.0
0.8
0.6
0.4
0.2
0.0
245 250 255 260 265 270 275
Surface Temperature (K)
SHEBA May–July 1998
b
Observed LWC (g/m**3)
1.0
0.8
0.6
0.4
0.2
0.0
245 250 255 260 265 270 275
Cloud–base Temperature (K)
SHEBA May–July 1998
c
Observed LWC (g/m**3)
1.0
0.8
0.6
0.4
0.2
0.0
245 250 255 260 265 270 275
Surface Temperature (K)
SHEBA May–July 1998
d
Observed LWC (g/m**3)
1.0
0.8
0.6
0.4
0.2
0.0
245 250 255 260 265 270 275
Cloud–base Temperature (K)

Fig. 5

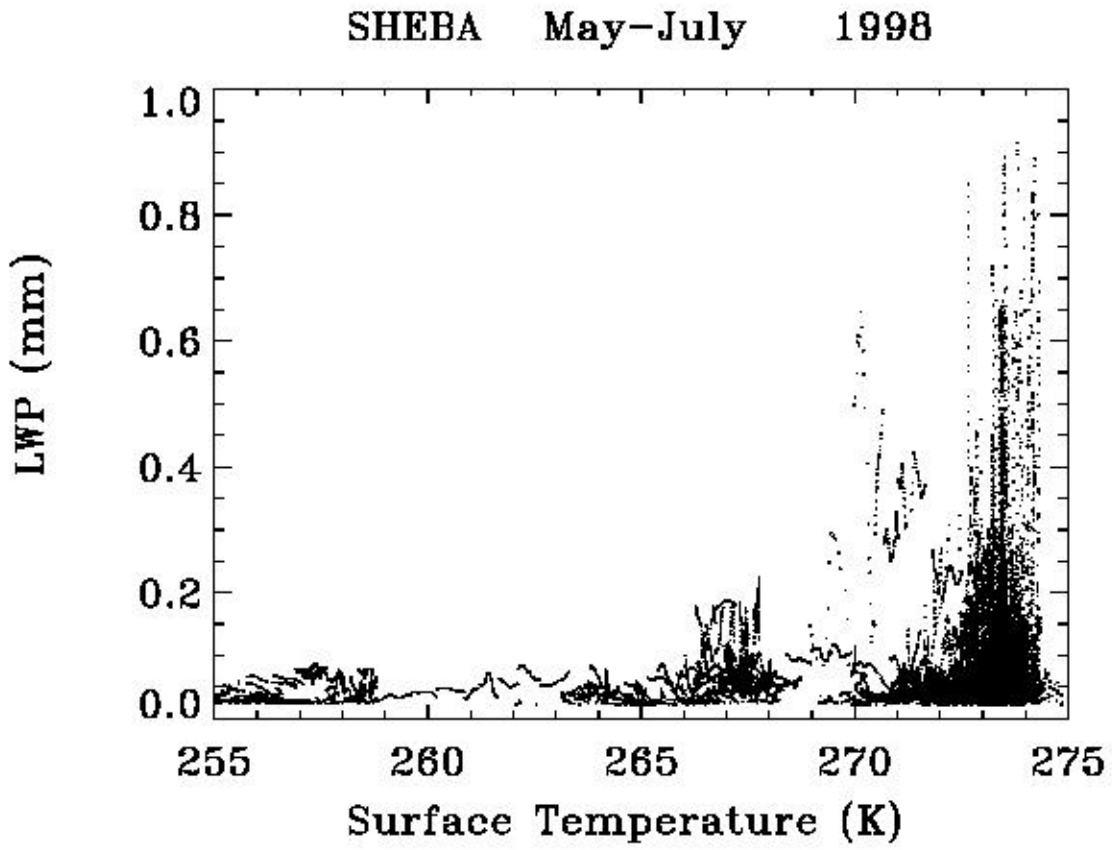
SHEBA May–July 1998
LWP (mm)
1.0
0.8
0.6
0.4
0.2
0.0
255
260
265
270
275
Surface Temperature (K)

Fig. 6

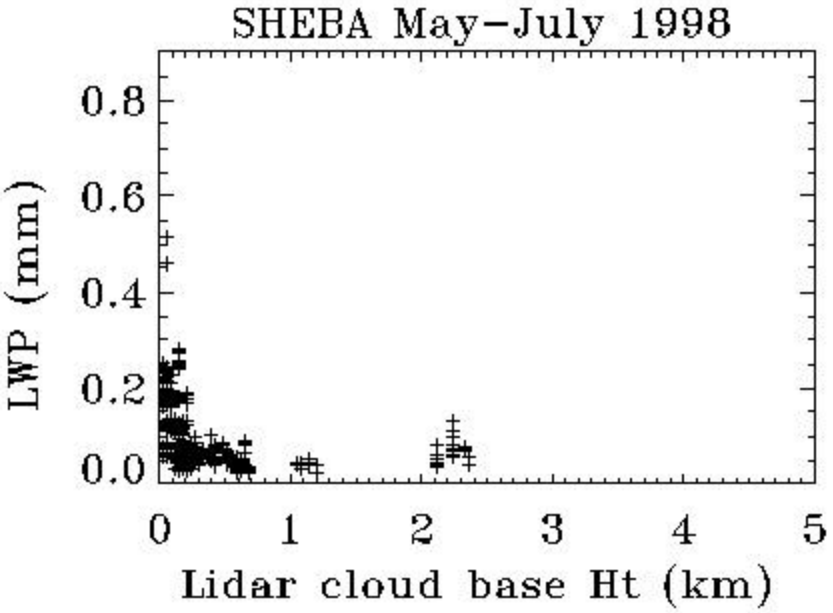
SHEBA May–July 1998
LWP (mm)
0.8
0.6
0.4
0.2
0.0
0
1
2
3
4
5
Lidar cloud base Ht (km)

Fig. 7

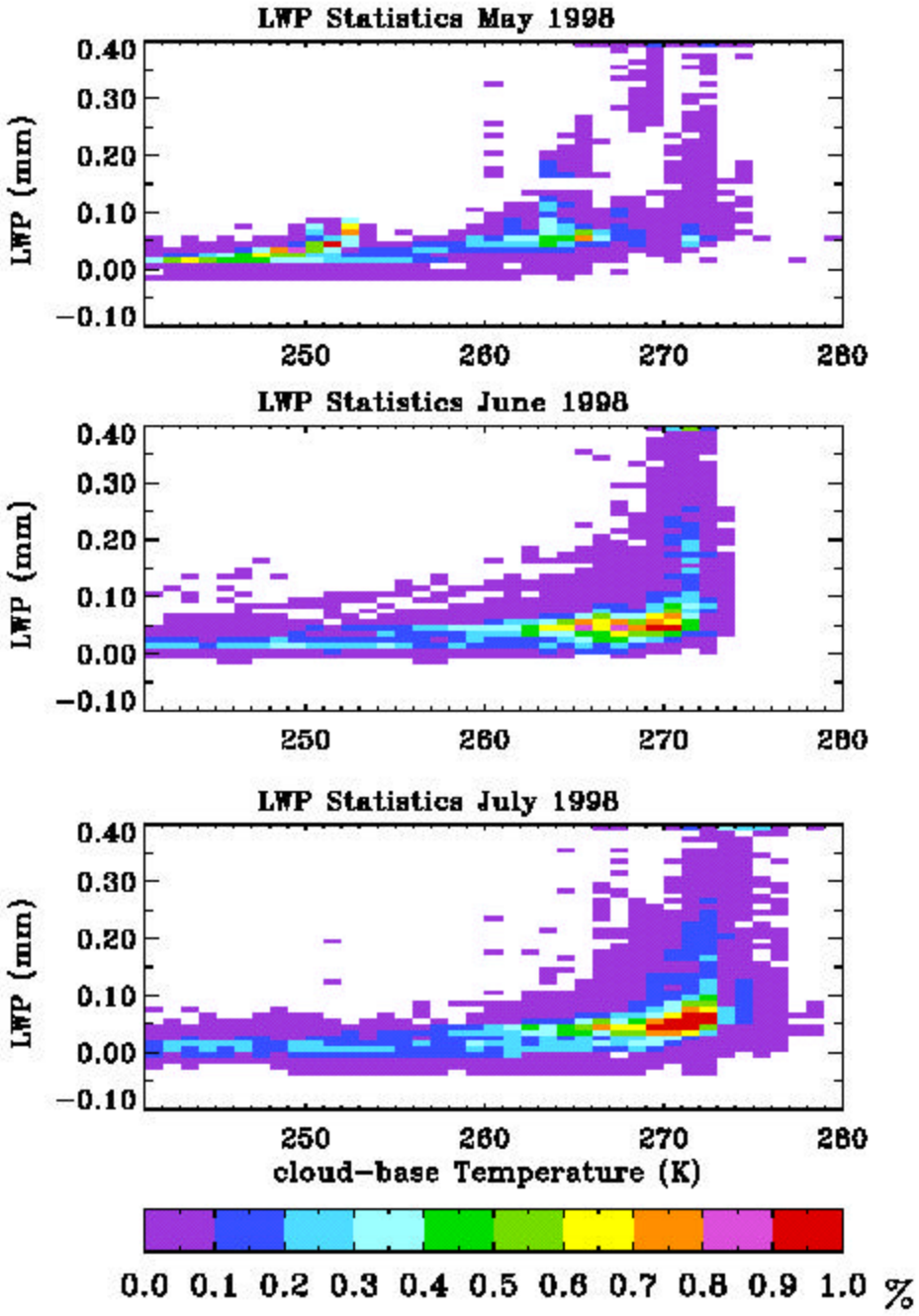
LWP Statistics May 1998
LWP (mm)
0.40
0.30
0.20
0.10
0.00
−0.10
250
260
270
280
LWP Statistics June 1998
LWP (mm)
0.40
0.30
0.20
0.10
0.00
−0.10
250
260
270
280
LWP Statistics July 1998
LWP (mm)
0.40
0.30
0.20
0.10
0.00
−0.10
250
260
270
280
cloud−base Temperature (K)
0.0 0.1 0.2 0.3 0.4 0.5 0.6 0.7 0.8 0.9 1.0 %

Fig. 8

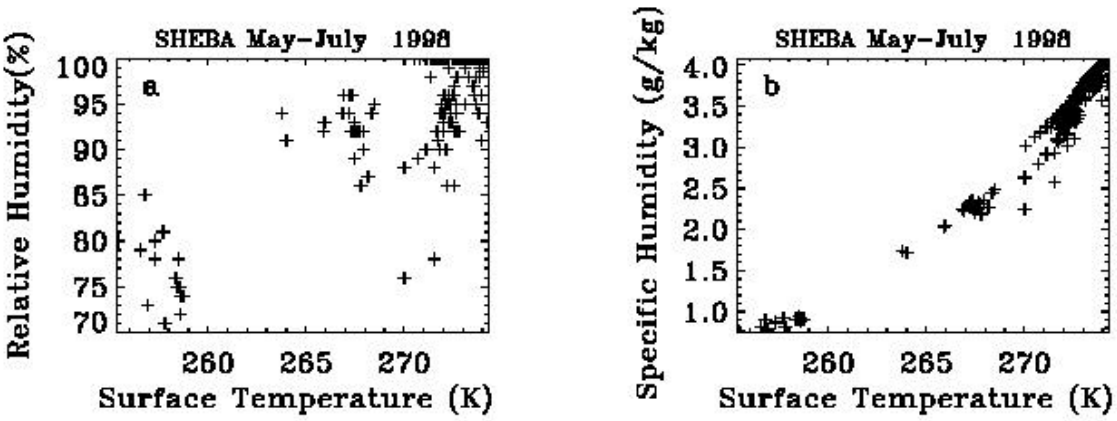
SHEBA May-July 1998
a
Relative Humidity(%)
100
95
90
85
80
75
70
260
265
270
Surface Temperature (K)
SHEBA May-July 1998
b
Specific Humidity (g/kg)
4.0
3.5
3.0
2.5
2.0
1.5
1.0
260
265
270
Surface Temperature (K)

Fig. 9

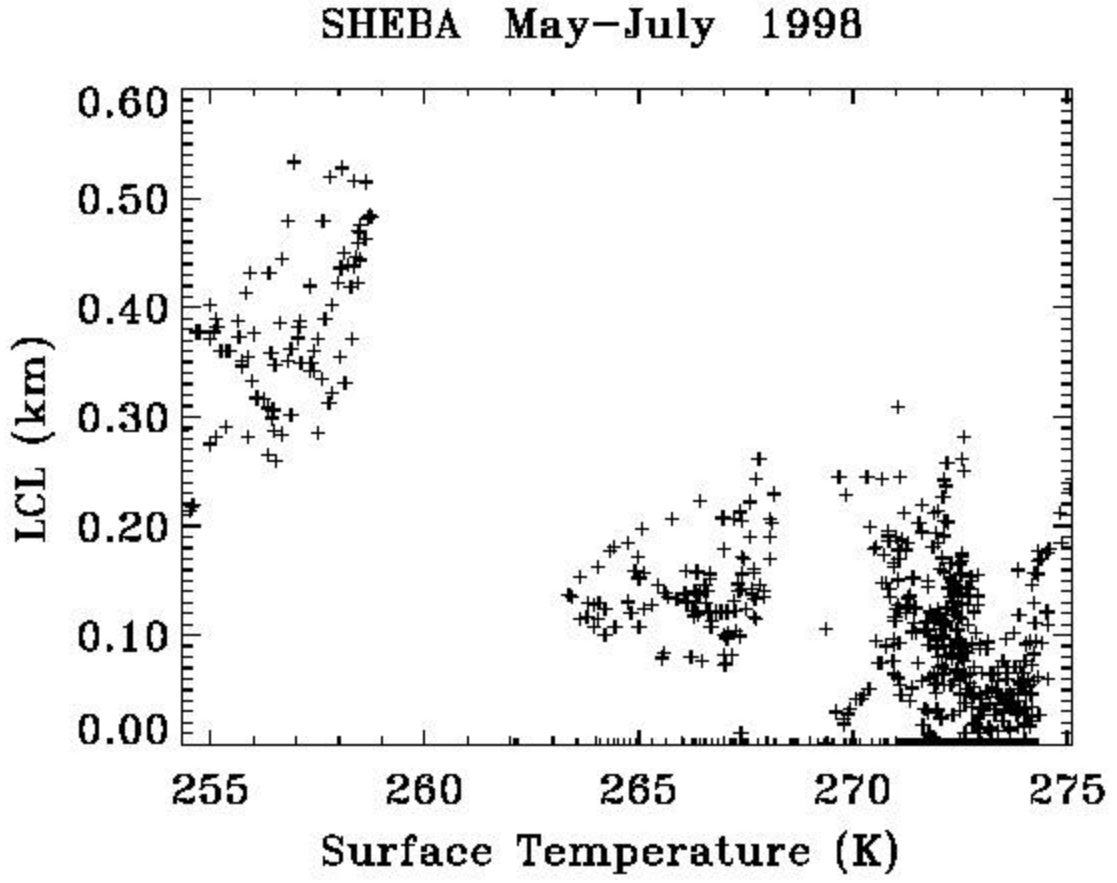
SHEBA May-July 1998
LCL (km)
0.60
0.50
0.40
0.30
0.20
0.10
0.00
255
260
265
270
275
Surface Temperature (K)

Fig. 10

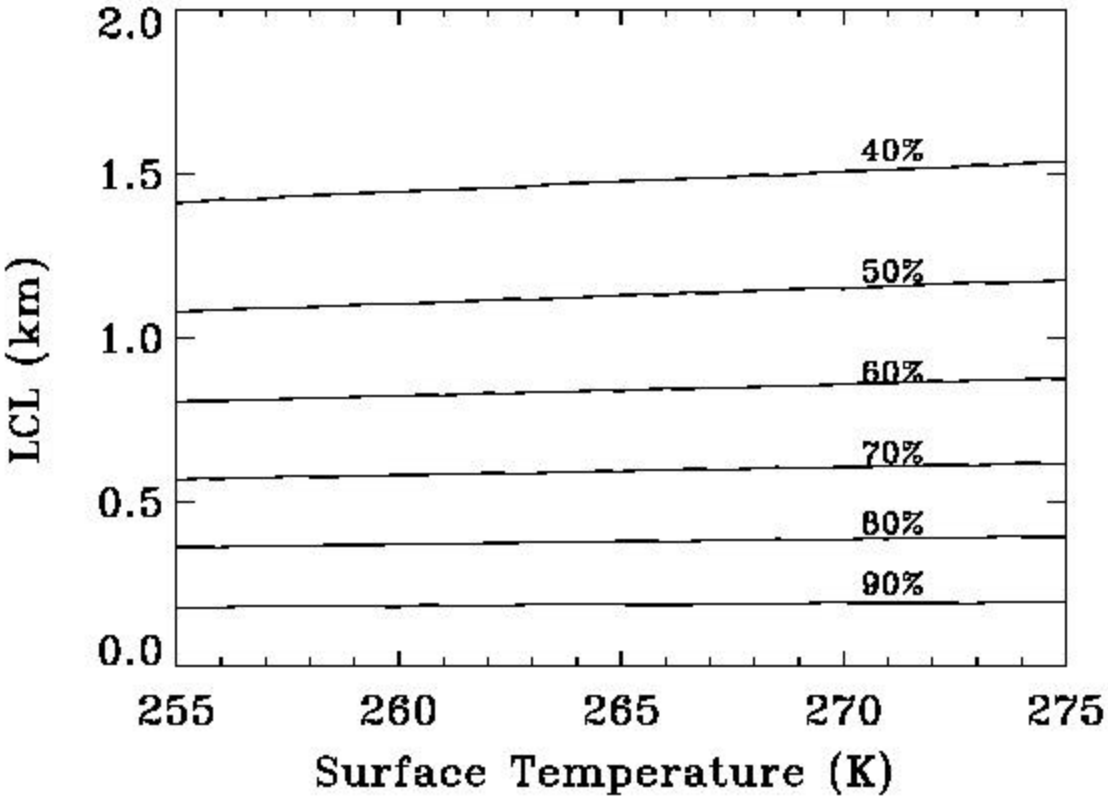
2.0
1.5
1.0
0.5
0.0
LCL (km)
40%
50%
60%
70%
80%
90%
255
260
265
270
275
Surface Temperature (K)

Fig. 11

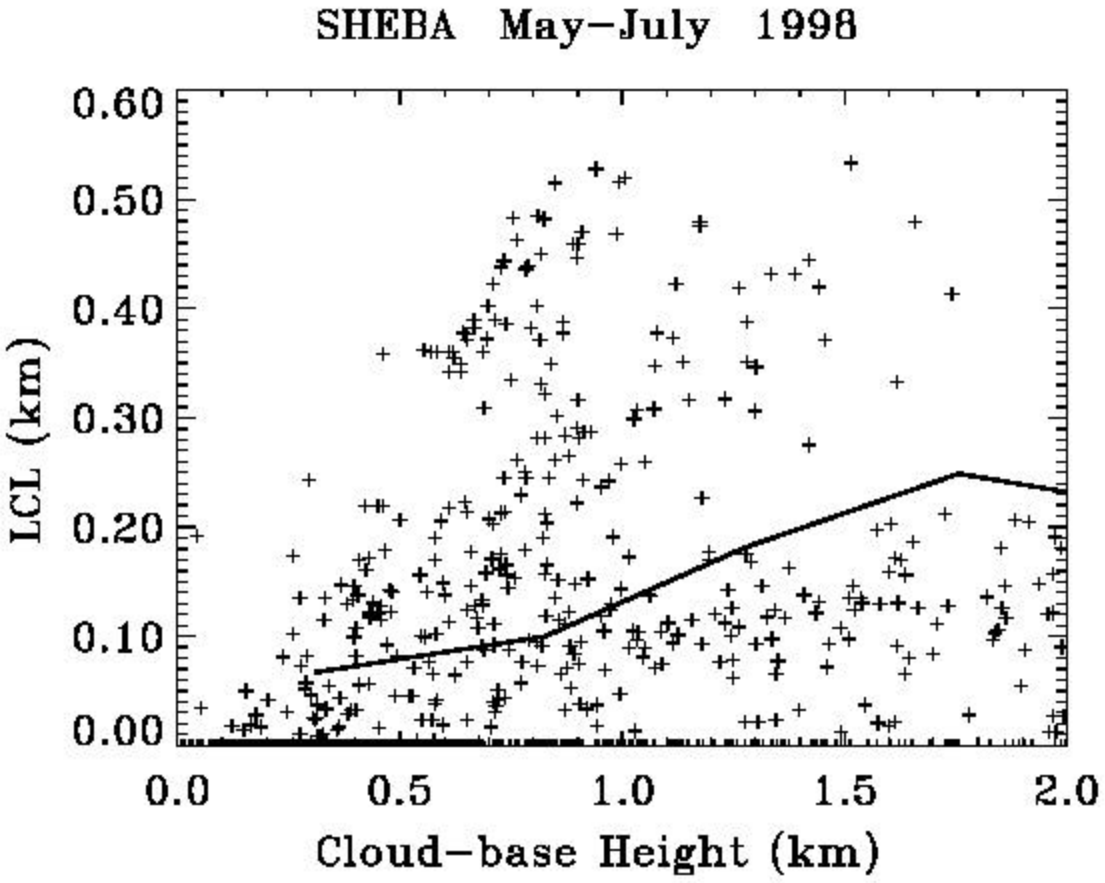
SHEBA May–July 1998
LCL (km)
0.60
0.50
0.40
0.30
0.20
0.10
0.00
0.0
0.5
1.0
1.5
2.0
Cloud–base Height (km)